City Research Online

City, University of London Institutional Repository

High sensitivity micro-fiber Mach-Zehnder interferometric temperature sensors with a high index ring layer

YUQI WU,[1] DONG YAN,[1] NAN-KUANG CHEN,[1,4] KENNETH T. V. GRATTAN,[2] B. M. A. RAHMAN,[2] XUAN LI,[3] ZHEN TIAN,[1] LIQIANG ZHANG,[1] XIA ZHANG,[1,5] XIAOGUANG ZHANG,[3] LIXIA XI,[3] AND HU ZHANG[3]

[1] *School of Physics Sciences and Information Technology, Liaocheng University, Liaocheng 252000, China*
[2] *Department of Electrical and Electronic Engineering, City, University of London, London, EC1 V 0HB, UK*
[3] *State Key Laboratory of Information Photonics and Optical Communications, Beijing University of Posts and Telecommunications, Beijing, China*
[4] *nankuang@gmail.com*
[5] *wenerzhang2002@163.com*

Abstract: The influence of the high index ring layer (HIRL) in a tapered fiber Mach-Zehnder interferometer (MZI) on the interference observed, and thus on its potential applications in temperature sensing, has been investigated. The MZI was comprised of a tapered Ring Core Fiber (RCF), spliced between two single mode fibers (SMF). Since part of core mode from the SMF was converted into cladding modes in the RCF, due to the mismatch in the cores between the RCF and SMF, the residual power enters and then propagates along the center of the RCF (silica). The difference in phase between the radiation travelling along these different paths is separated by the HIRL to generate an interference effect. Compared with fiber interferometers based on core and cladding mode interference, the thin fiber HIRL is capable of separating the high order cladding modes and the silica core mode, under grazing incident conditions. Therefore, the optical path difference (OPD) and the sensitivity are both substantially improved over what is seen in conventional devices, showing their potential for interferometric temperature sensor applications. The optimum temperature sensitivity obtained was 186.6 pm/°C, which is ~ 11.7 times higher than has been reported previously.

1. Introduction

Fiber optic interferometers are important components for communications systems, lasers, imaging and for optical fiber-based sensing systems. In recent years, device miniaturization has become an important issue for micro-fiber interferometric sensors: to improve the integration density of components and to provide better environmental stability. To achieve these goals, interference effects based on core-cladding or inter-core modes in fibers have been extensively studied [1–5]. Looking at the issue of miniaturization, the entire device length can be successfully decreased to a few hundred micrometers in size and the limit of detection for the liquid sample volume used can be decreased to the picoliter level, when used for refractive index and temperature sensing [2,3]. However, such microfiber interferometric sensors are not able to produce good extinction ratios and there is a limit in the sensitivity that is obtainable due to an insufficient Optical Path Difference (OPD) per unit length, when using a standard SMF. In general, the OPD in fiber interferometers can be optimized by selecting the most suitable numerical aperture (NA) of the fiber used, in that way to generate a larger OPD within a few hundred-micron length device length (or indeed even shorter lengths are possible). The high NA fibers can give rise to a

larger index difference between the core and cladding modes for a larger OPD, and thus higher sensitivity [2–3]. However, many unwanted cladding modes would also be excited, inducing more optical losses and resulting in spatial mode beating. This is unlikely to be good for linear and dynamic sensing over a wide spectral range, since the OPD is highly dependent on the mode orders [3].

By contrast, creating a HIRL in RCF is found to be a good method to efficiently increase the OPD per unit length by separating the core and high order cladding modes, to travel through different paths, as part of miniaturizing such fiber interferometers. The RCF has been intensively investigated in recent years with a view to enlarging the transmission capacity, this benefitting from the use of optical angular momentum (OAM) modes [6,7]. However, in the experiments described in this work, the excitation of the OAM modes is intentionally avoided so that the HIRL is used mainly to increase the OPD, and thus the sensitivity. To create the MZI, a short segment of RCF (of a few centimeters in length) is fusion-spliced between two SMFs, to form the interferometer in this way. The core mode of SMF splits into two parts at the first splicing point. One part is converted into the cladding modes, to propagate along the cladding surrounding the HIRL of the RCF (called the cladding mode), whereas the other part enters the silica center of the RCF (called the silica center mode). The two parts meet at the second splicing point to generate interference. To investigate the influence of the HIRL on the spectral interference and mode evolution, the central region of the RCF is immersed in a hydrogen flame and tapered to a thin HIRL. Normally, in a typical fiber optic, a low-index layer (such as fluorine-doped silica) is used preferentially to separate or depress some of the selected modes [8], this based on the total internal reflection effect. By contrast, a high-index layer is employed in this work to separate the core and cladding modes – however, this effect is only valid under grazing incidence conditions. It is interesting to note that for grazing incidence radiation travelling from a low index medium to a high index medium, the radiation will be reflected significantly [9]. Consequently, this HIRL can be used quite effectively to separate the core and cladding modes, to expand the OPD more efficiently when the core and cladding modes interfere with each other to generate interference at the second splicing point. Since the HIRL can only reflect the grazing incidence radiation, the core mode will be gradually coupled into the HIRL to generate the 'bottle beam' mode [10] or see a deterioration of the interference when the HIRL is continuously tapered and thus significantly thinned. However, there is a problem with the optical losses when the majority of the optical power is confined to propagate in the HIRL. In general, with the presence of the HIRL, it is advantageous to increase the OPD and its sensitivity or to convert the fiber core mode into the 'bottle beam' modes in microfiber interferometers. With the use of the HIRL, the temperature sensitivity can be improved and data shows that it is ∼ 11.7 times higher, at 186.6 pm/°C (for the silica fiber MZI), than has been seen from other, previous reports in the literature [1,11–22].

2. Working principle of the micro fiber Mach-Zehnder temperature sensors

A Ge-doped HIRL configured with a pure silica center (SC) is available as a RCF, where it was originally designed for use for OAM mode transmission [6,7]. The measured index profile of the RCF preform considered in this work is shown in Fig. 1, this being fabricated based on the MCVD/PCVD method. From Fig. 1, the central dip in the region, with a negative index difference, arises because of the presence of a collapsed air hole in the final stage of preparing the fiber preform. This then can locally reduce the refractive index for the fiber preforms made and based on MCVD method. However, when the preform is drawn into a fiber, the central index dip becomes negligible. This step-index RCF is then end-spliced to a single mode fiber (type SMF-28) and tapered to form a micro MZI with a HIRL, as shown schematically in Fig. 2. Before splicing it to the SMF, the HIRL is intentionally illuminated using a white light LED, with a source area of 1 mm × 1 mm, this being placed at the other end of a 1-m-long RCF and as illustrated in Fig. 3(a) (where the RCF is kept physically straight). After splicing to the SMF, it
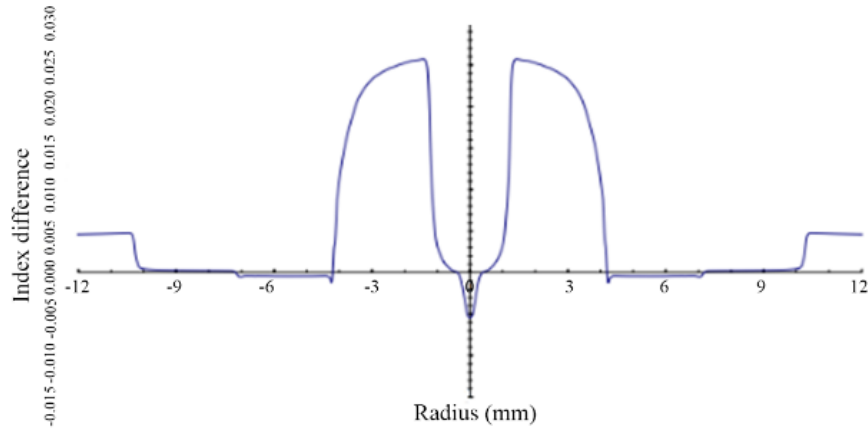
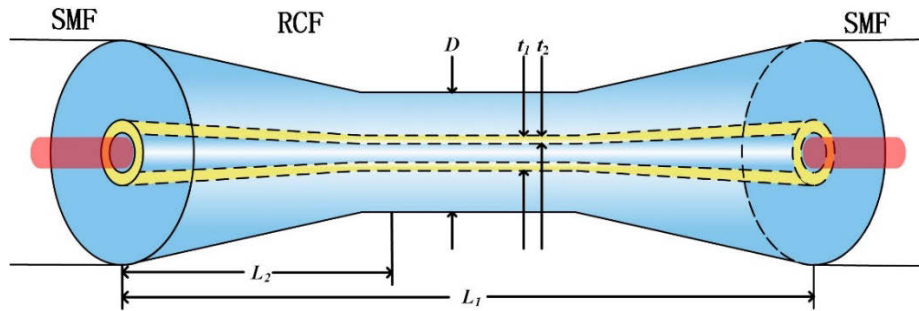**Fig. 1.** Measured index profile of RCF preform.

Fig. 2. Schematic diagram of the MZI comprising a tapered RCF. L_1: length of tapered RCF, L_2: length between left end of RCF and the cleaved point for mode patterns observation, D: diameter of tapered RCF, t_1: outer diameter of HIRL, t_2: thickness of HIRL.

can be seen from Fig. 3(b) that a fractional amount of the light from the core mode from the SMF is converted into cladding modes in the RCF (at the splicing point, due to the core-to-core mismatch). In addition, the residual power of the core mode from the SMF enters the silica center of the RCF and propagates as an SC mode, similarly to the fundamental core mode. The SC and the cladding modes encounter each other and produce interference at the second splicing point as a result. Assuming that the intensities of the SC mode and the cladding mode are I_{CS} and I_{CL}, respectively, the output intensity, I_{OC}, can be written as shown in Eq. (1) below:

$$I_O = I_{SC} + I_{CL} + 2\sqrt{I_{SC}I_{CL}} \cos\left[\frac{2\pi\Delta(nL)}{\lambda}\right] \qquad (1)$$

where λ is the operating wavelength and $\Delta(nL)$ is the OPD seen between the SC mode and the cladding mode. The original diameters for the core of the SMF, the SC of the RCF, the inner and outer diameters of the HIRL were 8.2 μm, 9.59 μm, 9.59 μm, and 15.76 μm, respectively. Since the core size of the SMF is smaller than that of the SC, the white light illumination from the LED enters the SC part, as the SC mode, and also excites several cladding modes at the first splicing point as can be seen from Fig. 3(b). It is evident that the HIRL plays a role in separating the core and cladding modes, because the light cannot be guided in this high index area. The grazing incident light beam is strongly reflected by the HIRL, when the radiation is incident from the lower-index silica cladding or the SC to the HIRL. Consequently, the OPD between the SC mode

and the cladding modes can rise for interference situations where there are higher extinction ratios.
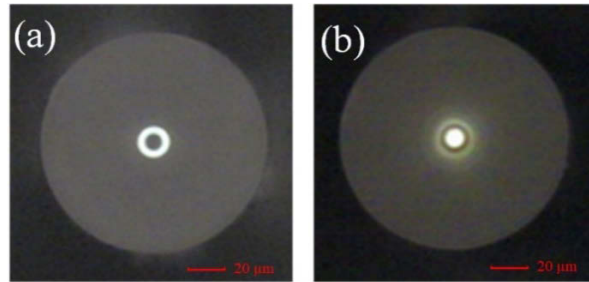
Fig. 3. Cross-sectional views of (a) the RCF and (b) the RCF spliced to the SMF when $L_2 = 7$ mm. The scale bars for 20 µm are shown in red in (a) and (b).

As discussed above, the grazing incident light beam (from the lower order cladding modes) cannot easy penetrate the HIRL to interfere with the SC mode. This implies that it will be much easier for the very high order cladding modes to interfere with the SC mode, by comparison to the situation with the lower order modes. Thus, the HIRL can stop the lower order cladding modes and allow the higher order cladding modes to interfere with the fundamental mode, an effect which has not previously been proposed. For the micro MZI created here, the SC mode is actually not a bound mode and thus can only survive over a short distance (in a range of a few tens of centimeters). However, this length is sufficient for making an effective interferometer. From Fig. 4(a), it can be seen that at the position just to the right of the splicing point, many cladding modes are excited, this resulting in chaotic interference fringes. However, the chaotic patterns quickly disappear after travelling a ~ 3 mm length and the clear circular interference fringes can thus be found in the cladding, as shown in Fig. 4(b). In Figs. 4(b)–4(f), the terms L_1, L_2, D, t_1 and t_2 stand for the length of the RCF, the distance between the (left-hand side) end of the RCF and the cleaved point (for the observation of the mode patterns), the tapered diameter of the MZI and the inner diameter and thickness of the HIRL, respectively. For sample A, the dark ring surrounding the SC mode is seen to be the HIRL in Figs. 4(b)–4(d). Through rigorous investigation, it can be confirmed that the majority of the light is not guided in the HIRL, due to grazing incidence. When the HIRL is heated and stretched by use of the hydrogen flame, t_2 gradually decreases – but it is still possible clearly to see the separation of the cladding and SC modes. For sample B, as t_2 is thinned down to 2.26 µm (with $t_1 = 9.72$ µm, $L_1 = 17$ mm, $L_2 = 8.5$ mm, and $D = 71.39$ µm), the SC mode is entirely coupled to the HIRL and no cladding modes can obviously survive, as is shown in Figs. 4(e)–4(f). From Figs. 4(b)–4(f), it is evident that the use of the HIRL is a satisfactory way to make the higher order cladding modes penetrate the HIRL more than the lower order modes, and thus a substantial improvement in the OPD is beneficial for achieving a better level of interference signal, and thus higher sensitivity. Thus, in summary, the working principle of the micro MZI is as follows. Initially, the single-mode light from the SMF is split into the SC mode and cladding modes, when entering the RCF, separated by the HIRL and passing along different optical paths. This produces an OPD between the SC mode and the lower order cladding modes, under the grazing incidence conditions. After travelling for a few millimeters, the lower order cladding modes interfere with the SC and when the RCF is further tapered, the HIRL is thinned down and the lower order cladding modes are eventually coupled and guided by the HIRL. The results of a simulation carried out for the 2- and 3-dimensional mode field distributions along the tapered RCF (carried out using BeamPROP software) are shown in Figs. 5(a)–5(c). The corresponding simulation parameters for L_1, t_1, and t_2 are as follows: ($L_1 = 5$ mm, $t_1 = 15.76$ µm, $t_2 = 3.08$ µm), ($L_1 = 7$ mm, $t_1 = 10.32$ µm, $t_2 = 2.35$

μm), and ($L_1 = 17$ mm, $t_1 = 9.1$ μm, $t_2 = 2$ μm), respectively. Even though Figs. 4(a)–4(f) show the mode patterns for the tapered RCF at different values of L_2, based on white light illumination, this can reflect the evolution of the propagation field distributions for operating wavelengths around 1550 nm. It also means that at a wavelength of ~1550 nm, the SC mode and cladding modes (seen in Figs. 5(a)–5(c)) are found to be separated by the HIRL first and then further are confined to propagate in the HIRL, when RCF is strongly tapered. Although the diameter of the SC is 9.59 μm (and this is slightly larger than the SMF-28 core), Fig. 4(g) (1000x magnification CCD microscope) shows the mode pattern at $L_2 = 3.5$ mm, which verifies that only the fundamental mode can be guided at SC and interference effects are involved. The photograph of the magnified core was taken using sample C, with the broadband light from the super-luminescent diodes used spanning the wavelength range 1250- 1650 nm, this being launched into the RCF, following which the mode patterns were observed. The silicon detectors in the CCD microscope used are sensitive below 1350 nm. Overall, for the MZI with $L_1 = 7$ mm, the best extinction ratio achieved is 7.87 dB, at 1558 nm. The best temperature sensitivity is 186.6 pm/°C, seen over the range
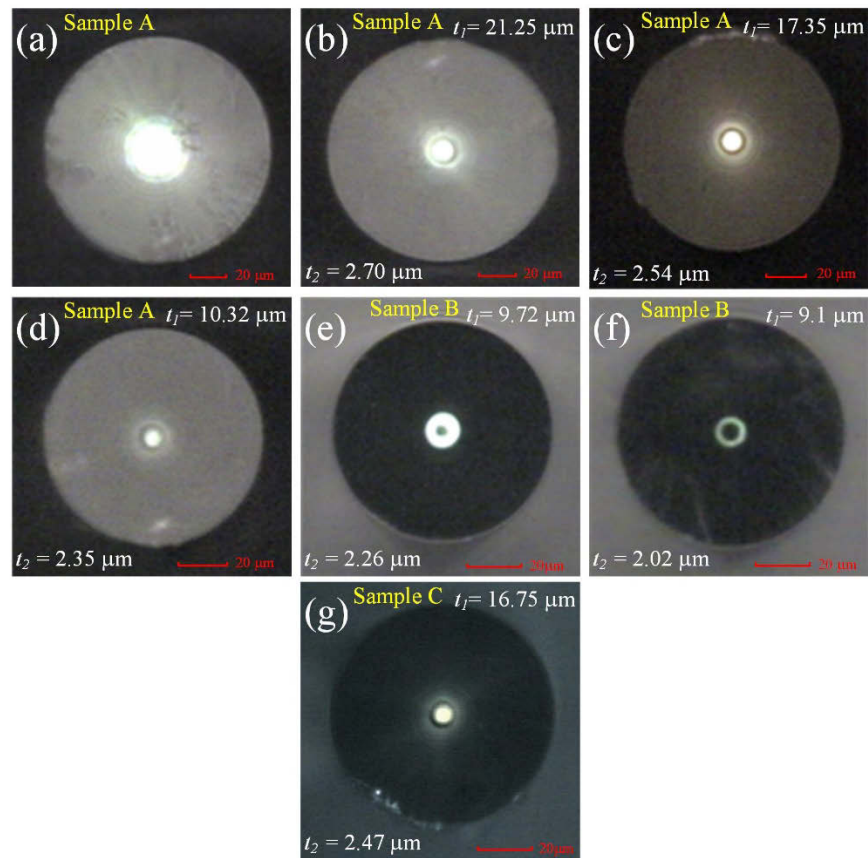
Fig. 4. (a) to (d): cross-sectional (1000X) CCD microphotograph of mode evolution for the MZI when L_2 is (a) 1, (b) 3, (c) 5 and (d) 7 mm using sample A ($L_1 = 7$ mm) illuminated by a white light LED; (e) to (f): cross-sectional (1000X) CCD microphotograph of MZI illuminated by a white light LED when D is (e) 74.56 μm, and (f) 70.73 μm while L_2 is 8.5 mm and 9.5 mm, respectively, using sample B ($L_1 = 17$ mm); (g) cross-sectional (1000X) CCD microphotograph of MZI illuminated by SLD lightsource using sample C ($L_1 = 7$ mm). The scale bars for 20 μm are shown in red from (a) to (g).

from 5°C to 25°C, this figure being ~ 11.7 times better than was seen from other previous reports [1,11–22]. In this way, the approach taken where the HIRL is used in this way is very promising for creating an effective improvement in the device sensitivity.
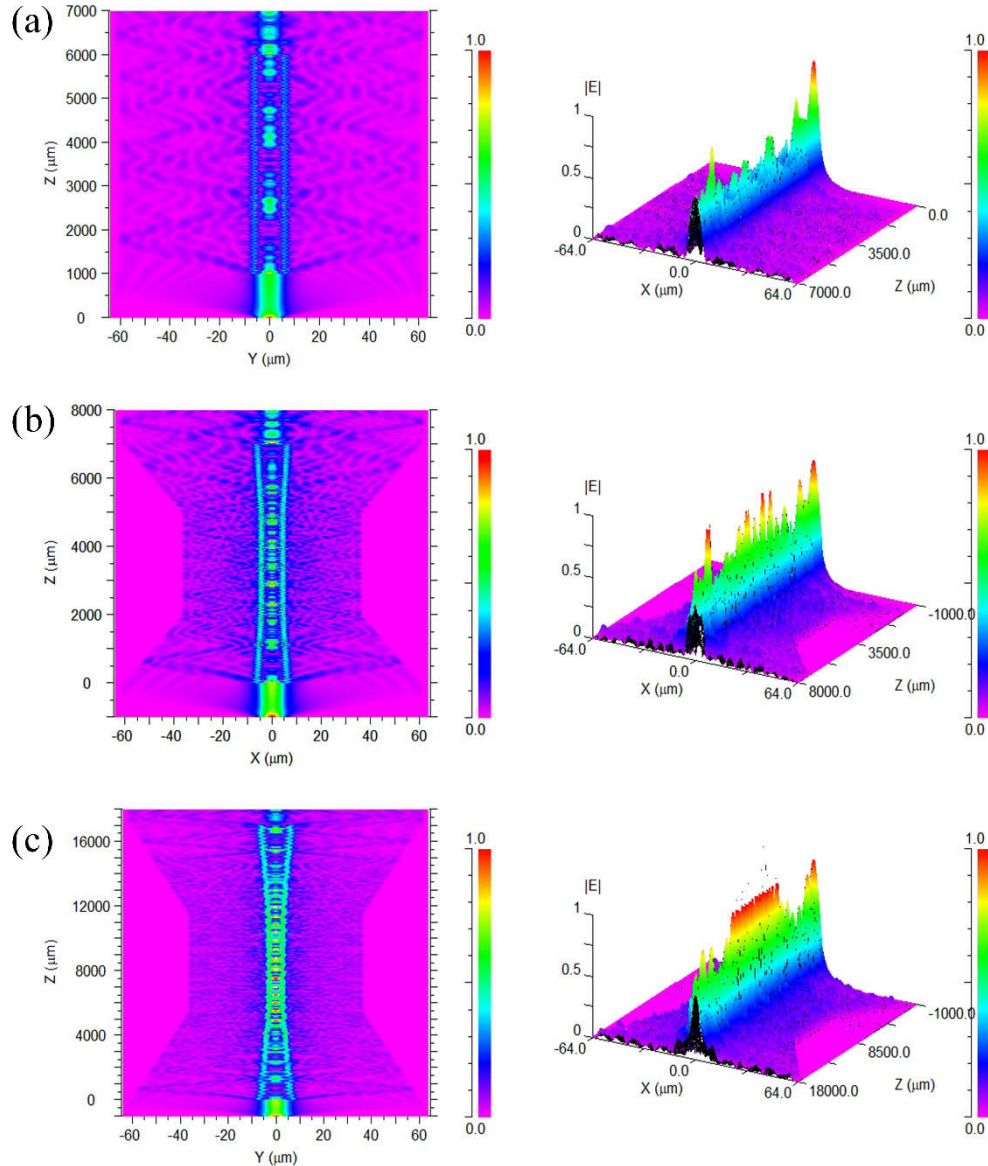
Fig. 5. Simulation results for the 2-dimensional (left) and 3-dimensional (right) mode field distributions along the RCF at 1550 nm wavelength, for the simulation parameters (a) $L_1 = 5$ mm, $t_1 = 15.76$ μm, $t_2 = 3.1$ μm, (b) $L_1 = 7$ mm, $t_1 = 10.32$ μm, $t_2 = 2.35$ μm, and (c) $L_1 = 17$ mm, $t_1 = 9.1$ μm, $t_2 = 2$ μm.

3. Experimental results and discussion

When used for measurement evaluations, radiation from a broadband SLD light source was launched into the MZI and the interference patterns were recorded by use of an Optical Spectrum

Analyzer (OSA), with an optical resolution of 0.05 nm. Figs. 6(a)–6(d) show the spectral responses of the MZI, comprising a tapered RCF with different values of D and L_1. It is evident that the clarity of the interference patterns deteriorates when L_1 is longer than 9 mm. The corresponding mode distribution is more like the situation seen in Fig. 4(d), where the mode patterns are not OAM modes (since the aim has been intentionally to avoid them being excited). From Fig. 4(d) and Fig. 6(a), it can be observed that the combination of an SC mode, together with a few cladding modes, can lead to the best conditions for observing the interference patterns. In Figs. 6(a)–6(b), the best extinction ratio achieved was 21.67 dB (at a wavelength of 1499 nm) when L_1 has a value of 23 mm. In Fig. 6(a), the multiple successive small ripples within the spectral range 1350-1450 nm were coming from the water vapor absorption in the hygroscopic monochromator of the OSA (Yokogawa: type AQ6370D), when used under high resolution. The Free Spectral Range (FSR) and the extinction ratios of the MZI respectively decreased and increased with increasing L_1, due to over-coupling and the accumulated OPD. In general, the insertion loss for the MZI was typically higher than 5 dB, especially at the shorter wavelengths. This arises because the mode field distribution between the SMF and the RCF was so different that chaotic mode patterns were therefore expected, as shown in Fig. 4(a). This phenomenon could be further alleviated by using a mode converter. The most important issue in this work has been experimentally to investigate and verify the influence of the HIRL on the OPD and the sensitivity of fiber MZI.
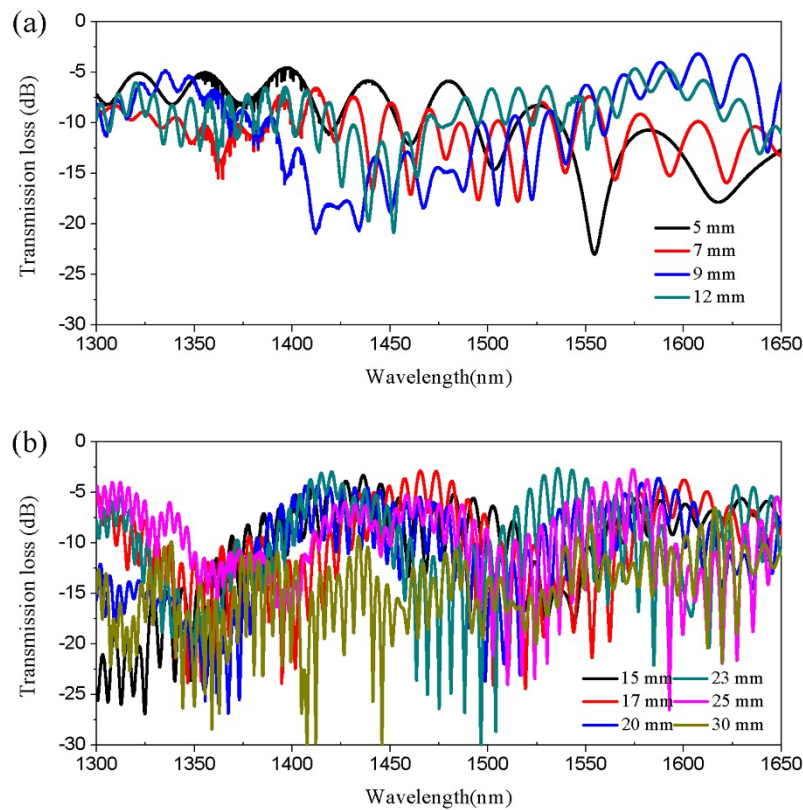
Fig. 6. (a)-(b) Spectral responses of the MZI at different values of L_1.

The spectral responses for the MZI, with ambient temperature variations, are shown in Figs. 7(a)–7(c) over the temperature ranges 5°C to 75°C. Figure 8 shows two linear fits of the
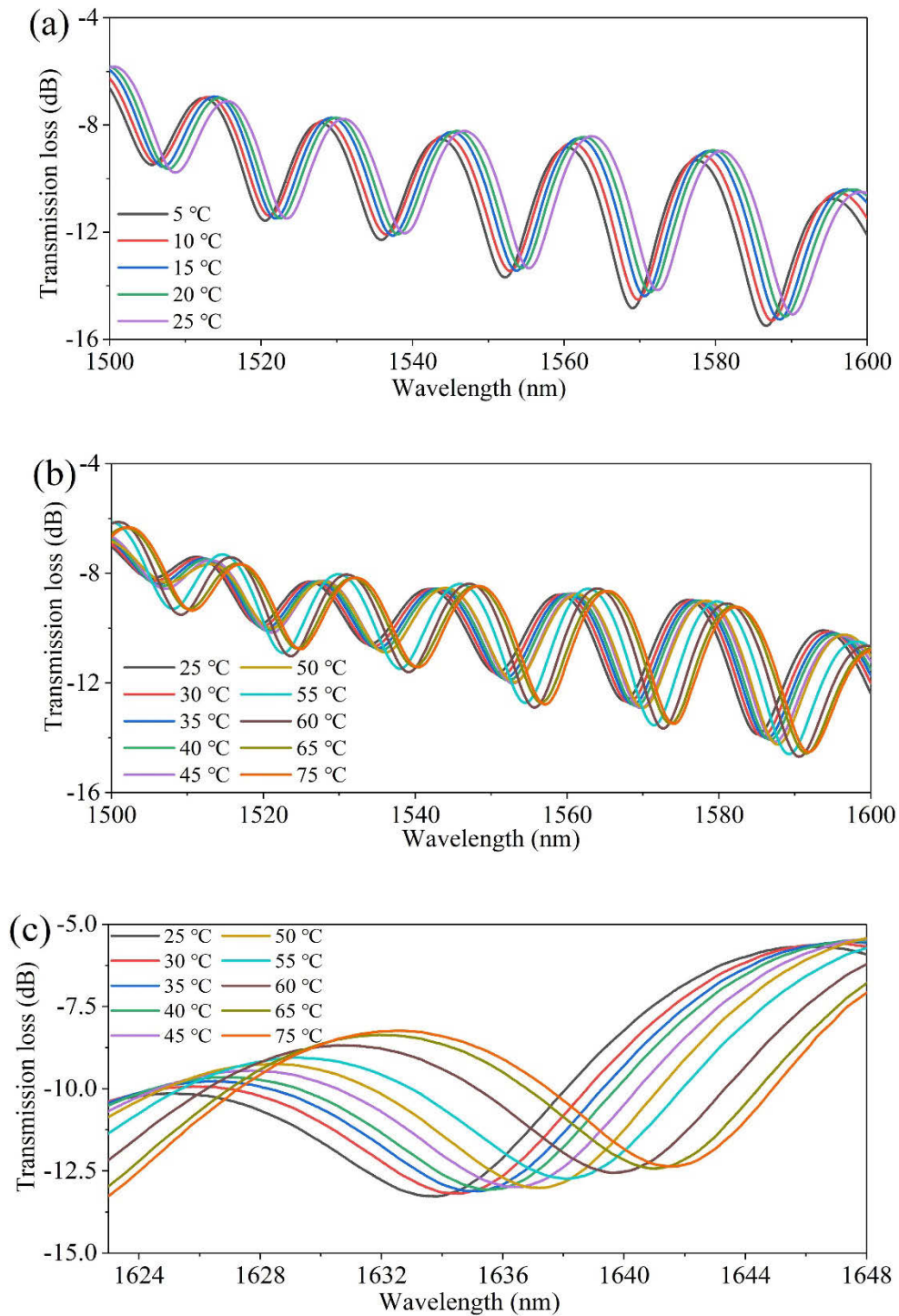
Fig. 7. Spectral responses of the temperature variations for $L_1 = 7$ mm over (a) 5°C - 25°C, (b) 25°C - 75°C and (c) "zoom-in'' for the spectral range over the wavelength range 1623-1648 nm.

wavelength shifts due to temperature variations at different values of L_1 over that temperature ranges (i) from 5°C to 25°C and (ii) from 25°C to 75°C, respectively. Given the limitations of the various temperature controllers used, these two regions can be seen as follows: Fig. 7(a) shows the cooling for MZI from ambient temperature and Figs. 7(b)–7(c), the heating from room temperature. For sample A, when the temperature, T, increases, the wavelength red-shifts for $L_1 = 7$ mm and the best extinction ratio obtained was 7.87 dB, at 1588 nm. The calculated temperature sensitivities, in accordance with the slopes of linear fits in Fig. 8, were 186.6 pm/°C and 171.9 pm/°C for temperature ranges 5°C - 25°C and 25°C - 75°C, respectively. The results are significantly higher than were seen in other, previous work published in the literature [1,11–22]. Hence, the optimum thickness of t_2 can be estimated to be ~ 2.35 μm, (as can be seen from Fig. 4(d), when $D = 72.58$ μm and $L_1 = 7$ mm), achieving higher sensitivity. This implies that by correctly controlling the values of t_1, t_2, L_1, and D, the sensitivity can be greatly improved and the influence of this HIRL is thus clearly verified, as being able further to enhance the sensitivity in the fiber MZI illustrated. To improve the sensitivity in the future, it is important to enlarge further the accumulated OPD rapidly between the SC mode and the cladding modes. Therefore, for the SC mode and a specific cladding mode, appropriately choosing those materials with a larger difference between their thermo-optic coefficients or increasing the optical length difference, e.g. selecting a very high order cladding mode, is a highly promising way to achieve the higher temperature sensitivity desired.
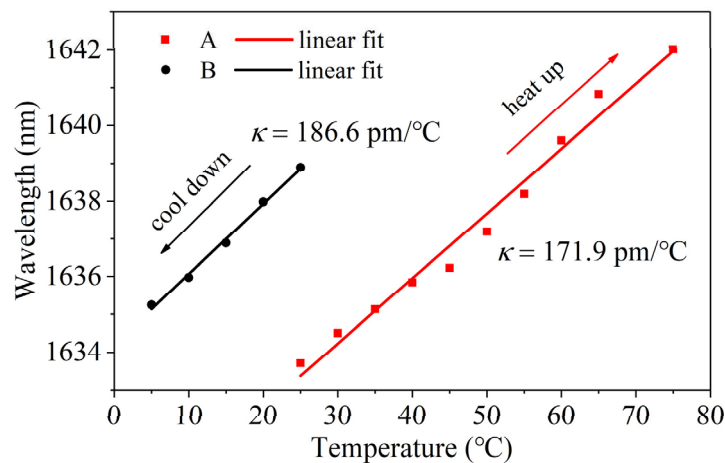
Fig. 8. Linear fits for the wavelength shift over the temperature range from 5°C - 25°C and 25°C - 75°C, respectively, using different temperature controlling devices to heat up and cool down.

4. Conclusions

A high sensitivity, microfiber MZI sensor system with a high-index ring core structure using a short ring core fiber has been demonstrated and its performance evaluated. The ring core structure was found to be effective in reflecting the grazing incidence radiation to separate the silica core mode and the higher order cladding modes, to increase the OPD and thus the device sensitivity. By using a 7-mm-long tapered RCF, the best extinction ratio achieved was 7.87 dB and the optimum temperature sensitivity observed has been improved over that reported in the literature to 186.6 pm/°C (over the temperature range 5°C to 25°C), this by a factor 11.7, important for silica fiber interferometric temperature sensors. The thickness of the high-index ring core, the diameter of the silica core and the length of the RCF are crucial factors in optimizing the performance. It

is clear that such a high-index ring core structure is helpful to separate the core mode and the cladding modes, to improve significantly the temperature sensitivity for silica fiber based MZIs. An over-tapered RCF can be used to convert the silica core mode into 'bottle beam' modes which then can be used potential applications in fiber lasers, such as optical tweezers.

Funding

Acknowledgment

Disclosures

The authors declare no conflicts of interest.

References

1. P. Chen, X. Shu, and K. Sugden, "Ultra-compact all-in-fiber-core Mach–Zehnder interferometer," Opt. Lett. **42**(20), 4059–4062 (2017).
2. N. K. Chen, S. H. Lo, C. L. Tsai, S. Kumar, W. H. Cheng, and R. Kashyap, "Towards picoliter microsensing in index and temperature using hundreds-micron-scale fiber Michelson interferometers," *CLEO:2017*, San Jose, CA (2017). paper no. JTh2A.112.
3. N. K. Chen, K. Y. Lu, and Y. H. Chang, "Wavelength-beat integrated micro Michelson fiber interferometer based on core-cladding mode interferences for real-time moving direction determination," *CLEO: 2013*, San Jose, CA, 2013, paper no. ATh4 K.5.
4. O. Yaghobi and H. R. Karimi-Alavijeh, "Single step process for optical microfiber in-line Mach-Zehnder interferometers fabrication," IEEE Photonics Technol. Lett. **30**(10), 915–918 (2018).
5. Z. Tian and S. S. H. Yam, "In-line single-mode optical fiber interferometric refractive index sensors," J. Lightwave Technol. **27**(13), 2296–2306 (2009).
6. H. Yan, S. Li, Z. Xie, X. Zheng, C. Du, and B. Zhou, "Chromatic dispersion diagnosis of three OAM states in 5.58 kilometer ring-core fiber link," IEEE Photonics J. **9**(3), 1–7 (2017).
7. C. Brunet, B. Ung, L. Wang, Y. Messaddeq, S. LaRochelle, and L. A. Rusch, "Design of a family of ring-core fibers for OAM transmission studies," Opt. Express **23**(8), 10553–10563 (2015).
8. K. Takahashi, T. Ishigure, and Y. Koike, "Index profile design for high-bandwidth W-shaped plastic optical fiber," J. Lightwave Technol. **24**(7), 2867–2876 (2006).
9. Ghatak, *Optics* (Fourth Edition). Tata McGraw-Hill, New Delhi, India, Ch. 24.1-24.3 (2009).
10. M. D. Wei, W. L. Shiao, and Y. T. Lin, "Adjustable generation of bottle and hollow beams using an axicon," Opt. Commun. **248**(1-3), 7–14 (2005).
11. P. Chen, X. Shu, and K. Sugden, "Compact assembly-free vector bend sensor based on all-in-fiber-core Mach–Zehnder interferometer," Opt. Lett. **43**(3), 531–534 (2018).
12. W. W. Li, D. N. Wang, Z. K. Wang, and B. Xu, "Fiber in-line Mach-Zehnder interferometer based on a pair of short sections of waveguide," Opt. Express **26**(9), 11496–11502 (2018).
13. J. Harris, P. Lu, H. Larocque, Y. Xu, L. Chen, and X. Bao, "Highly sensitive in-fiber interferometric refractometer with temperature and axial strain compensation," Opt. Express **21**(8), 9996–10009 (2013).
14. Y. Zhao, F. Xia, H. F. Hu, and C. Du, "A ring-core optical fiber sensor with asymmetric LPG for highly sensitive temperature measurement," IEEE Trans. Instrum. Meas. **66**(12), 3378–3386 (2017).
15. L. Li, L. Xia, Z. Xie, and D. Liu, "All-fiber Mach-Zehnder interferometers for sensing applications," Opt. Express **20**(10), 11109–11120 (2012).
16. B. Yin, M. Wang, S. Wu, Y. Tang, S. Feng, Y. Wu, and H. Zhang, "Fiber ring laser based on MMF-PMFBG-MMF filter for three parameters sensing," Opt. Express **25**(25), 30946–30955 (2017).
17. H. Bae, D. Yun, H. Liu, D. A. Olson, and M. Yu, "Hybrid miniature Fabry–Perot sensor with dual optical cavities for simultaneous pressure and temperature measurements," J. Lightwave Technol. **32**(8), 1585–1593 (2014).
18. Z. Zhu, L. Liu, Z. Liu, Y. Zhang, and Y. Zhang, "Surface-plasmon-resonance-based optical-fiber temperature sensor with high sensitivity and high figure of merit," Opt. Lett. **42**(15), 2948–2951 (2017).
19. G. Liu, M. Han, and W. Hou, "High-resolution and fast-response fiber-optic temperature sensor using silicon Fabry-Pérot cavity," Opt. Express **23**(6), 7237–7247 (2015).
20. A. Tapetado, P. J. Pinzón, J. Zubia, and C. Vázquez, "Polymer optical fiber temperature sensor with dual-wavelength compensation of power fluctuations," J. Lightwave Technol. **33**(13), 2716–2723 (2015).

21. Y. Jiang, Z. Fang, Y. Du, E. Lewis, G. Farrell, and P. Wang, "Highly sensitive temperature sensor using packaged optical microfiber coupler filled with liquids," Opt. Express **26**(1), 356–366 (2018).
22. S. Weng, L. Pei, J. Wang, T. Ning, and J. Li, "High sensitivity D-shaped hole fiber temperature sensor based on surface plasmon resonance with liquid filling," Photonics Res. **5**(2), 103–107 (2017).